Stem Cell Reports
Report

ISSCR

OPEN ACCESS

SCA-1 Expression Level Identifies Quiescent Hematopoietic Stem and Progenitor Cells

Mina N.F. Morcos,[1] Kristina B. Schoedel,[1] Anja Hoppe,[1] Rayk Behrendt,[1] Onur Basak,[2] Hans C. Clevers,[2,3] Axel Roers,[1] and Alexander Gerbaulet[1,*]

[1]Institute for Immunology, Faculty of Medicine, TU Dresden, Fetscherstrasse 74, 01307 Dresden, Germany
[2]Hubrecht Institute, Royal Netherlands Academy of Arts and Sciences (KNAW) and University Medical Center Utrecht
[3]Princess Máxima Centre
3584 CT Utrecht, the Netherlands
*Correspondence: alexander.gerbaulet@tu-dresden.de
http://dx.doi.org/10.1016/j.stemcr.2017.04.012

SUMMARY

Blood cell generation depends on continuous cellular output by the sequential hierarchy of hematopoietic stem cell (HSC) and progenitor populations that all contain quiescent and actively cycling cells. Hematopoietic stem and progenitor cells (HSPCs) express the surface molecule Stem cell antigen 1 (SCA-1/LY6A). Using histone 2B-red fluorescent fusion protein label retention and cell-cycle reporter mice, we demonstrate that high SCA-1 expression (SCA-1^{hi}) identifies not only quiescent HSCs but quiescent cells on all hierarchical levels within the lineage$^-$SCA-1$^+$KIT$^+$ (LSK) population. Each transplanted SCA-1^{hi} HSPC population also displayed self-renewal potential superior to that of the respective SCA-1^{lo} population. SCA-1 expression is inducible by type I interferon (IFN). We show, however, that quiescence and high self-renewal capacity of cells with brighter SCA-1 expression at steady state were independent of type I IFN signaling. We conclude that SCA-1 expression levels can be used to prospectively isolate functionally heterogeneous HSPC subpopulations.

INTRODUCTION

The multi-potent and self-renewing hematopoietic stem cells (HSCs) at the top of the hierarchy give rise to hematopoietic progenitor cell (HPC) populations with gradually narrowing differentiation and self-renewal potential (Eaves, 2015). Murine HSCs and uncommitted progenitors express the glycosyl phosphatidylinositol-anchored cell surface protein Stem cell antigen 1 (SCA-1/LY6A) (Holmes and Stanford, 2007) and reside within the lineage$^-$SCA-1$^+$KIT$^+$ (LSK) population (Okada et al., 1992; Purton and Scadden, 2007; Spangrude et al., 1988) of the bone marrow (BM).

Numerous studies have demonstrated heterogeneity within each of the hematopoietic stem and progenitor cell (HSPC) populations with regard to cell-cycle activity (Wilson et al., 2008), lineage specification (Dykstra et al., 2007; Müller-Sieburg et al., 2002), and repopulation activity (Foudi et al., 2008; Qiu et al., 2014). Multiple cell-surface markers allowing for prospective isolation of the quiescent subset of HSCs (Balazs et al., 2006; Grinenko et al., 2014; Kiel et al., 2005; Osawa et al., 1996; Shin et al., 2014; Sudo et al., 2012) have been proposed. However, a marker uniformly associated with quiescence among the LSK population has been lacking so far. Two recent studies (Säwén et al., 2016; Wilson et al., 2015) showed increased quiescence and repopulation activity of immunophenotypic HSCs with high expression of SCA-1 (SCA-1^{hi}).

While the function of the SCA-1 molecule remains enigmatic (Holmes and Stanford, 2007), it is well established that SCA-1 is strongly upregulated by type I (Essers et al., 2009; Pietras et al., 2014) and type II (de Bruin et al., 2014) interferon (IFN). SCA-1 seems to regulate cellular responses to type I IFN as loss of SCA-1 abrogates type I IFN-induced proliferation of HSCs (Essers et al., 2009; Walter et al., 2015).

In the present work, we show that type I IFN-independent high expression of SCA-1 identifies quiescent cells with elevated repopulation activity not only in the HSC compartment but also in LSK progenitor populations.

RESULTS

High SCA-1 Expression Identifies Quiescent Cells Not Only in HSCs but Also in Progenitor Populations

To identify the most quiescent HSPCs, we induced expression of histone 2B-red fluorescent fusion protein (H2B-RFP) by doxycycline (DOX) treatment of *R26^{rtTA}/Col1A1$^{H2B\text{-}RFP}$* mice (Egli et al., 2007) for 8 weeks and analyzed the BM after different chase periods for retention of H2B-RFP by flow cytometry (Figures S1A and S1B). In accordance with previous studies (Foudi et al., 2008; Qiu et al., 2014; Säwén et al., 2016; Wilson et al., 2008), we observed rapid dilution of H2B-RFP from HPCs (HPC-1, LSK CD48^{hi}CD150$^-$, HPC-2, LSK CD48^{hi}CD150$^+$) (Oguro et al., 2013) (see Figure S1C for gating), while a proportion of the HSC (LSK CD48$^{-/lo}$CD150$^+$) and multipotent progenitor (MPP) populations (LSK CD48$^{-/lo}$CD150$^-$) (Kiel et al., 2005) retained the label for up to 19 weeks (see Figure S1D). We compared the expression of surface antigens between quiescent H2B-RFP$^+$ cells and their respective parental populations. Most

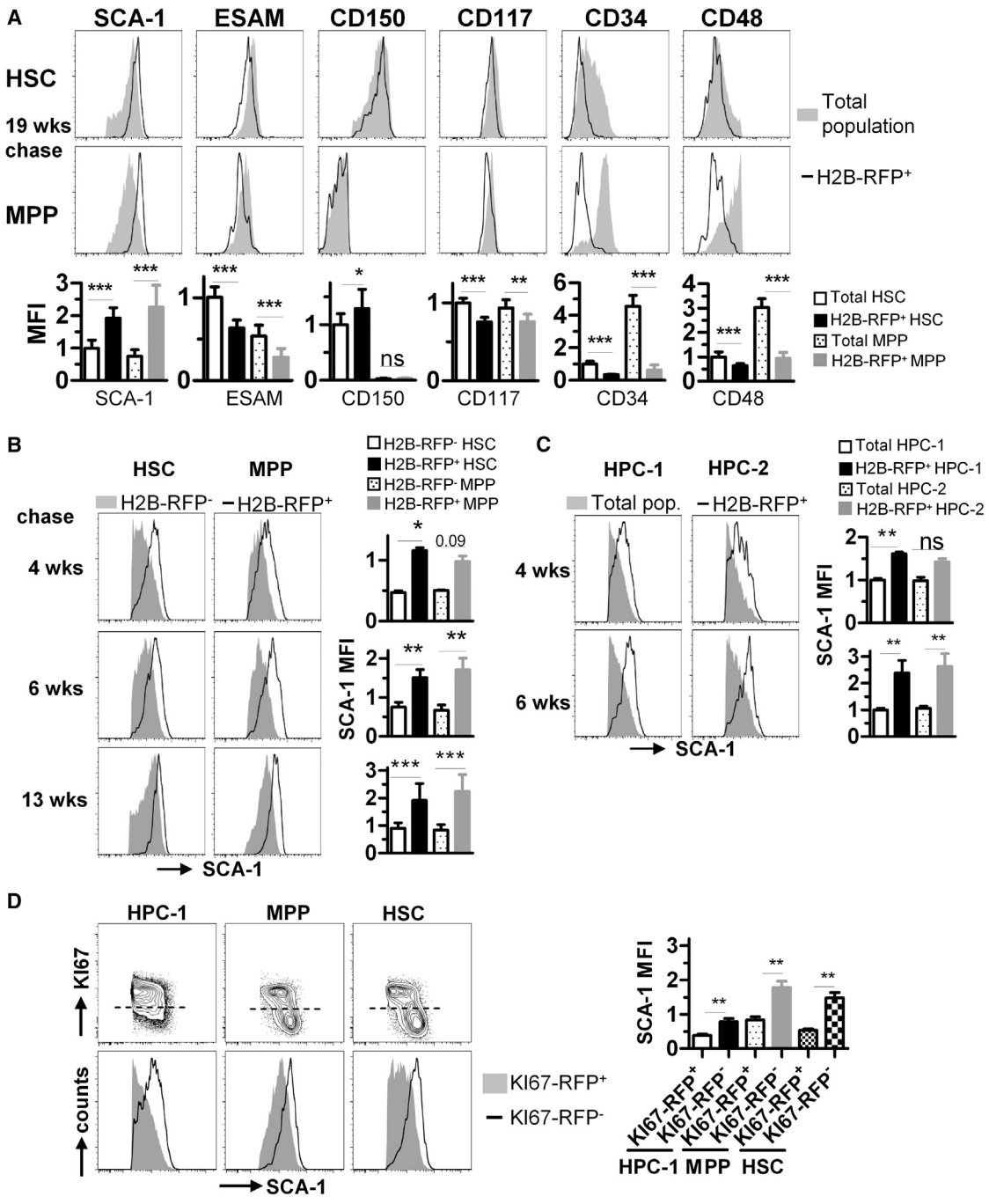

Figure 1. Quiescent Hematopoietic Stem and Progenitor Cells Express High Levels of SCA-1

(A–C) *R26*^{rtTA}/*Col1A1*$^{H2B\text{-}RFP}$ mice were DOX-pulsed, chased for either 4, 6, 13, or 19 weeks, and HSPC populations were analyzed by flow cytometry for retention of H2B-RFP (see also Figures S1A–S1D). (A) Representative histograms of BM HSCs (LSK CD48$^{-/lo}$CD150^{+}, upper row) or MPPs (LSK CD48$^{-/lo}$CD150^{-}, middle row) from mice (n = 9) chased for 19 weeks are shown. H2B-RFP^{+} label retaining cells (black lines) were overlaid on to the total parental population (solid gray histograms). Antigen median fluorescence intensities (MFI, lower row, normalized to the mean MFI of HSCs) of the total or H2B-RFP^{+} populations were determined and compared. (B) Representative histograms for SCA-1 expression of BM HSCs (left column) and MPPs (middle column) isolated from *R26*^{rtTA}/*Col1A1*$^{H2B\text{-}RFP}$ mice chased for either 4 (upper row, n = 2), 6 (middle row, n = 4), or 13 weeks (lower row, n = 8) are shown and H2B-RFP^{+} (black lines) and H2B-RFP^{-} cells (solid gray histograms) were overlaid. SCA-1 MFIs (right column, normalized to total HSC population) of H2B-RFP^{-} and H2B-RFP^{+} HSPCs were compared. (C) Representative SCA-1 expression histograms of BM HPC-1 (LSK CD48^{hi}CD150^{-}, left column) or HPC-2 cells (LSK

(legend continued on next page)

prominently, we observed significantly higher expression of SCA-1 on label-retaining HSCs and MPPs after 4, 6, 13, and 19 weeks of chase (Figures 1A and 1B). Moreover, elevated SCA-1 expression was also detectable in both H2B-RFP$^+$ HPC populations after 4 and 6 weeks of chase (Figure 1C). In addition, we found a significant down-regulation of endothelial cell-specific adhesion molecule (ESAM) (Yokota et al., 2008), CD117 (Grinenko et al., 2014; Shin et al., 2014), CD34, and CD48 (Qiu et al., 2014) on 19-week label-retaining HSCs and MPPs, while CD150 (Beerman et al., 2010; Kiel et al., 2005; Morita et al., 2010) was slightly, but significantly, upregulated on H2B-RFP$^+$ HSCs (Figure 1A).

Next, we analyzed the BM of *Ki67-RFP$^{ki/wt}$* cell-cycle reporter mice (Basak et al., 2014), in which a KI67-RFP fusion protein faithfully reports quiescent (KI67-RFP$^-$) and cycling (KI67-RFP$^+$) HSPCs (Figure S1E). RFP expression did not alter hematopoiesis in this model as judged by HSPC compartment size and competitive transplantation (Figures S1F and S1G). Cells with bright SCA-1 expression were significantly enriched among quiescent KI67-RFP$^-$ HPC-1, MPP, and HSC populations, while cycling KI67-RFP$^+$ HSPCs expressed lower SCA-1 levels (Figure 1D).

To identify alternative markers of HSPC quiescence, we correlated expression of CD201 (EPCR) and CD27 (Balazs et al., 2006; Vazquez et al., 2015; Wiesmann et al., 2000) to SCA-1 and KI67-RFP expression (Figures S1H and S1I). We found CD201 expression level to be extremely useful for prospective enrichment of KI67-RFP$^-$ HSPCs, and expression of CD201 and SCA-1 showed a strong positive correlation. In contrast, CD27 expression appeared to be independent of cell-cycle activity and SCA-1. We did not observe any link between ESAM and KI67-RFP expression among HSCs, as the latter uniformly expressed a high level of ESAM (Figure S1J), while ESAM expression was heterogeneous among HPC-1 and MPP and without correlation to KI67-RFP expression.

SCA-1^{hi} HSPCs Have High Repopulation Activity upon Transplantation

To investigate whether repopulation activity of donor HSPCs correlates with SCA-1 expression, we fractionated HSCs, MPPs, and HPCs-1 into either SCA-1^{hi} or SCA-1^{lo} populations (Figure S2A) and competitively transplanted these cells into lethally irradiated congenic recipients (Figure 2A). We observed a range of SCA-1 fluorescence intensity of approximately two decades among BM LSK cells and arbitrarily divided these SCA-1$^+$ cells into two populations, in which the SCA-1^{lo} fraction comprised events from the lower decade, while the SCA-1^{hi} fraction consisted of events from the higher decade. The sorting gates were placed to discriminate SCA-1-negative outliers as well as avoiding overlap between SCA-1^{lo} and SCA-1^{hi} populations after sorting (Figures S2A and S2B).

SCA-1^{hi} donor HSCs displayed durable multi-lineage repopulation of recipient peripheral blood (PB) and BM (Figure 2B, columns I and II; Figures S2B–S2D), while SCA-1^{lo} HSCs either contributed to a much lower extent in primary (Figure 2B) and secondary recipients (Figure S2E) or were devoid of long-term and serial repopulation activity (Figure S2D). In contrast to HSCs, SCA-1^{hi} MPPs did not harbor stable multi-lineage repopulation potential as evidenced either by a decline in PB neutrophil and BM chimerism at 16 weeks after transplantation (Figure 2C, columns I and II) or by secondary transplantation (Figure S2E). However, the intermediate-term repopulation of all leukocyte lineages by transplanted SCA-1^{hi} MPPs was significantly enhanced compared with SCA-1^{lo} donor MPPs. Likewise, SCA-1^{hi} donor HPC-1 cells exhibited significantly elevated B-cell chimerism 3 weeks after transplantation in contrast to the corresponding SCA-1^{lo} population (Figure 2D, column I).

The comparison of SCA-1 expression among donor-derived (CD45.2$^+$) BM cells isolated from primary recipients of SCA-1^{hi} or SCA-1^{lo} donor cells (B6 HSCs or MPPs) revealed that SCA-1^{lo} donor cells or their progeny can reacquire high expression of SCA-1 (Figures 2B and 2C, columns III and IV; Figure S2F).

Higher SCA-1 Expression and Increased Repopulation Activity of Quiescent HSCs Does Not Depend on Type I IFN Signaling

SCA-1 expression is strongly upregulated by type I IFN (Essers et al., 2009), and *Ifnar1$^{del/del}$* mice, which lack type I IFN signaling (Kamphuis et al., 2006), showed on average

CD48^{hi}CD150$^+$, middle column) from *R26^{rtTA}/Col1A1$^{H2B\text{-}RFP}$* mice (as in B) are shown. H2B-RFP$^+$ populations (black lines) were overlaid onto the respective parental population (solid gray histograms). SCA-1 MFI (right column, mean MFI of total HPC-1 set to 1) of total and H2B-RFP$^+$ populations was calculated.

(D) BM of *Ki67-RFP$^{ki/wt}$* mice (n = 4, see also Figures S1E–S1G) was analyzed by flow cytometry. Representative contour plots of HPCs-1, MPPs, and HSCs are shown (upper row; dotted line shows threshold for KI67-RFP gating, set according to *Ki67-RFP$^{wt/wt}$* control). Lower row compares SCA-1 expression between KI67-RFP$^+$ cells (solid gray histograms) and KI67-RFP$^-$ (black lines) cells among the respective parental population. Right data plot quantifies SCA-1 MFI of HSPC populations separated by KI67-RFP expression. SCA-1 MFI was normalized to the mean MFI of the total HSC population, which was set to 1.

Means ± SD are shown throughout the figure. Significance was calculated by paired Student's t test and Bonferroni-Holm error correction for multiple testing. *p = 0.01–0.05, **p = 0.001–0.01, ***p < 0.001; ns, not significant. See also Figure S1.

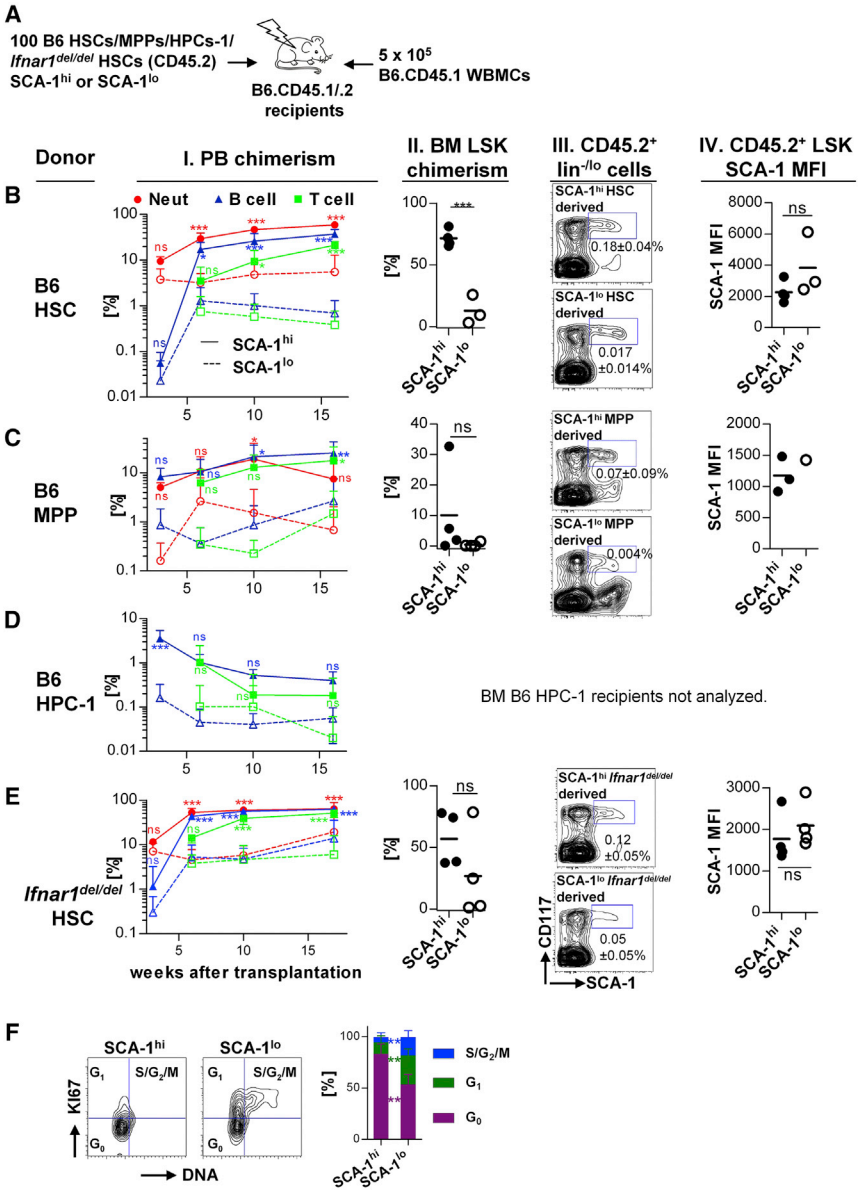

Figure 2. Type I IFN-Independent SCA-1 Expression Predicts Repopulation Activity

(A) HSPCs (either HSCs, MPPs, or HPCs-1 isolated from B6 mice or *Ifnar1*$^{del/del}$ HSCs, all CD45.2^{+}) were fractionated according to SCA-1 expression (see Figure S2A) and 100 cells were transplanted together with 5 × 10^{5} B6.CD45.1 competitor WBMCs into lethally irradiated B6.CD45.1/.2 recipients.

(B–E) Each row shows analysis of primary recipient mice transplanted with either B6 HSCs, B6 MPPs, B6 HPCs-1, or *Ifnar1*$^{del/del}$ HSCs (n = 3–4/group). (Column I) PB chimerism of recipient mice was monitored longitudinally (red circles, neutrophils; blue triangles, B cells; green boxes, T cells. Continuous line, filled symbols: SCA-1^{hi} donor cells; dotted line, open symbols: SCA-1^{lo} donor cells. Means ± SD are shown, significance calculated with repeated-measures two-way ANOVA with Bonferroni error correction). (Column II) BM analysis of recipient mice revealed LSK donor chimerism (individual recipients and means are shown, unpaired Student's t test, BM chimerism of B6 HPC-1 recipients was not analyzed due to complete lack of PB neutrophil reconstitution). (Column III) Representative contour plots of donor-derived (CD45.2^{+}) lin$^{-/lo}$ cells are depicted. Frequency (mean ± SD) of the CD45.2^{+} LSK population among total WBMCs is shown. (Column IV) SCA-1 MFI of CD45.2^{+} LSK cells was calculated (individual recipients and means are shown, mice showing <0.001% of CD45.2^{+} LSK cells among total WBMCs were excluded from analysis, unpaired Student's t test). *p = 0.01–0.05, **p = 0.001–0.01, ***p < 0.001; ns, not significant.

(F) Representative contour plots of cell-cycle analysis of either SCA-1^{hi} or SCA-1^{lo} BM LSK cells isolated from *Ifnar1*$^{del/del}$ mice (n = 5). Right data plot shows frequencies of LSK cells in G_0, G_1, or $S/G_2/M$ phase (mean ± SD, paired Student's t test with Bonferroni-Holm error correction). **p = 0.001–0.01.

See also Figure S2.

decreased steady-state SCA-1 expression, albeit similar maximum levels (Figure S2G). The frequency of LSK cells was reduced in *Ifnar1*$^{del/del}$ mice, but the frequency as well as cell-cycle activity of HSCs was unchanged in comparison with control mice. However, there was still heterogeneity of SCA-1 expression levels within the various LSK HSPC populations of *Ifnar1*$^{del/del}$ mice. To investigate whether the superior repopulation activity of SCA-1^{hi} HSPCs depends on type I IFN, we competitively transplanted either SCA-1^{hi} or SCA-1^{lo} *Ifnar1*$^{del/del}$ HSCs (Figure S2A). The PB repopulation activity of SCA-1^{hi} *Ifnar1*$^{del/del}$ donor HSCs was significantly elevated compared with their SCA-1^{lo} counterparts (Figure 2E, column I). However, the chimerism level of SCA-1^{lo} *Ifnar1*$^{del/del}$ recipients started to rise at the end of primary transplantation (Figure 2E, columns I and II) and upon secondary transplantation (Figure S2E, columns I and II). SCA-1^{lo} *Ifnar1*$^{del/del}$ derived LSK cells of recipients showed reacquisition of bright SCA-1 expression (Figures 2E and S2E, columns III and IV). At the end of secondary transplantation, PB and BM chimerism as well as SCA-1 expression of both donor cell entities were indistinguishable (Figure S2E, columns I-IV). However, as

recipients of SCA-1^{hi} *Ifnar1*$^{del/del}$ donor HSCs displayed significantly higher PB chimerism throughout primary transplantation and in the initial phase of secondary transplantation, we conclude that constitutive type I IFN signaling does not account for the superior repopulation potential of HSPCs with high SCA-1 expression. Moreover, cell-cycle analysis of LSK cells from *Ifnar1*$^{del/del}$ mice corroborated our finding that the increased quiescence of SCA-1^{hi} HSPCs was type I IFN independent (Figure 2F).

DISCUSSION

We showed that high SCA-1 expression allows for prospective isolation of quiescent and potent hematopoietic progenitor cells. As previously reported, transplanted LSK CD48$^{-/lo}$CD150^{-} MPPs did not exhibit long-term reconstitution, but showed robust intermediate-term contribution to all blood cell lineages (Oguro et al., 2013). We showed that the vast majority of this repopulation potential was confined to those cells which expressed the highest levels of SCA-1 within the MPP population. These cells were rarely dividing in situ, as evidenced by label retention characteristics similar to those of SCA-1^{hi} HSCs as previously reported (Foudi et al., 2008; Säwén et al., 2016). Likewise, the B-lymphoid potential of the HPC-1 population was strongly enhanced among SCA-1^{hi} cells. In addition, we confirmed the recent finding (Säwén et al., 2016; Wilson et al., 2015) that the majority of functional HSCs resided within the SCA-1^{hi} LSK CD48$^{-/lo}$CD150^{+} population, while HSCs seemed to be rare or weak among those cells expressing lower amounts of SCA-1. However, SCA-1^{lo} donor cells could give rise to progeny with a SCA-1^{hi} phenotype, demonstrating plasticity of SCA-1 expression levels.

The BM lin^{-}CD201^{+}CD27^{+} population significantly overlaps with LSK cells in B6 mice and consists of early HSPCs. Lin^{-}CD201^{+}CD27^{+} cells have been proposed for alternative HSPC identification in mouse strains (e.g., BALB/c or NOD strains) or under stress conditions, which lack a distinct LSK immunophenotype (Vazquez et al., 2015). Our result that CD201 expression level correlates with quiescence of HSPCs similar to SCA-1 facilitates identification and isolation of quiescent subsets among lin^{-}CD201^{+}CD27^{+} HSPCs.

In contrast, ESAM, which was proposed to label HSCs under stress conditions in a cell-cycle-specific manner (Sudo et al., 2012), did not seem to be useful for prospective enrichment of quiescent HSPCs at steady state, as KI67-RFP and ESAM expression showed poor correlation.

We demonstrate that the properties of SCA-1^{hi} cell populations were not a result of constitutive type I IFN signaling. The latter was surprising, as steady-state type I IFN partially accounted for SCA-1 expression (Figure S2G) and "tonic" (basal or constitutive) type I IFN signaling has been implied in HSC maintenance (Gough et al., 2012). However, our transplantation data revealed that SCA-1^{hi} as well as SCA-1^{lo} *Ifnar1*$^{del/del}$ HSCs outgrew wild-type (wt) competitor cells in secondary recipients, which may be explained either by a general competitive advantage of *Ifnar1*$^{del/del}$ HSCs over wt competitor HSCs or, due to lower overall SCA-1 expression in *Ifnar1*$^{del/del}$ mice, potent HSCs still reside in the SCA-1^{lo} sorted population. The latter is very likely, as our SCA-1 sorting strategy for *Ifnar1*$^{del/del}$ donor cells separated only the brightest fraction of HSCs into the SCA-1^{hi} subset, while SCA-1^{lo} cells contained the majority of the cell population. Nevertheless, purified SCA-1^{hi} *Ifnar1*$^{del/del}$ donor cells repopulated primary recipients faster and more robustly. Moreover, cell-cycle analysis of *Ifnar1*$^{del/del}$ HSPCs revealed that the increased quiescence of the SCA-1^{hi} population was type I IFN independent.

Hematopoietic contribution, differentiation pattern, and the relationship between the HSPC subpopulations and diverse SCA-1 expression have not been addressed in situ so far. We speculate that discrepancies between recent studies reporting high (Sawai et al., 2016) or low (Busch et al., 2015; Schoedel et al., 2016; Sun et al., 2014) contribution of HSCs to steady-state hematopoiesis might reflect lineage tracing of exclusive HSC subpopulations that differ by SCA-1 expression and cell-cycle activity.

SCA-1 is already one of the most widely used markers for prospective isolation of murine HSPCs, and our finding that quiescent subpopulations are identified by differential SCA-1 expression easily allows for refined purification and analysis strategies.

EXPERIMENTAL PROCEDURES

Mice

C57Bl/6 wt, B6.CD45.1, B6CD45.1/.2, *Ifnar1*$^{del/del}$ (Kamphuis et al., 2006), *R26*^{rtTA}/*Col1A1*$^{H2B\text{-}RFP}$ (Egli et al., 2007) and *Ki67-RFP*$^{ki/wt}$ (Basak et al., 2014) mice were housed at the Experimental Center, TU Dresden. *R26*^{rtTA}/*Col1A1*$^{H2B\text{-}RFP}$ mice were induced by drinking water containing 1 mg/mL doxycycline (Applichem) and 1% sucrose ad libitum for 8 weeks.

All animal experiments were carried out in accordance with institutional guidelines and were approved by Landesdirektion Dresden Ref. No. 24-9168.11-1/2012-39.

Cell Preparation

Whole bone marrow cells (WBMCs) were isolated by crushing long bones with mortar and pestle using PBS/2% fetal calf serum (FCS)/2 mM EDTA and filtered through a 100-μm mesh. After erythrocyte lysis in NH_4Cl buffer, cells were filtered through a 40-μm mesh. Hematopoietic lineage^{+} cells were removed with the lineage cell depletion kit (Miltenyi Biotec).

PB was drawn by retrobulbar puncture.

BM Transfer

B6.CD45.1/.2 recipient mice received a single dose of 9 Gy of total body irradiation (Yxlon Maxi Shot Source). Donor cells (purified CD45.2$^+$ test cells mixed with B6.CD45.1 competitor WBMCs) were administered via intravenous injection into the retro-orbital sinus. For secondary transplantation, equal numbers of WBMCs from all primary transplanted individuals were pooled and 4 × 10^6 cells were transplanted into each lethally irradiated secondary recipient.

Flow Cytometry

Cells were stained for 30 min with fluorochrome-labeled antibodies (see Table S1) diluted in PBS/2% FCS/2 mM EDTA, washed twice, and analyzed or sorted on BD FACSAria or Miltenyi MACSquant flow cytometers. Data were analyzed using FlowJo 9.9.4 (Treestar). Negative and positive populations were identified by fluorescence-minus-one (FMO) controls. For gating of H2B-RFP$^+$ and H2B-RFP$^-$ HSPC populations, the respective population from uninduced *R26*^{rtTA}/*Col1A1*$^{H2B\text{-}RFP}$ mice served as background H2B-RFP controls. KI67-RFP$^+$ and KI67-RFP$^-$ HSPCs were identified using antibody-stained HSPCs from *Ki67-RFP*$^{wt/wt}$ animals as negative controls.

For cell-cycle analysis, cells were incubated with antibodies against extracellular markers, fixated/permeabilized (BD Cytofix/Cytoperm kit), and intracellularly stained with anti-KI67 and FxCycle Violet DNA stain (Thermo Fisher Scientific). KI67$^-$ cells were gated according to FMO isotype controls.

Statistical Analysis

Statistical analysis was conducted with Prism 5 (GraphPad). Significance of results is indicated in the figures by *p = 0.01–0.05, **p = 0.001–0.01, ***p < 0.001, and ns (not significant).

SUPPLEMENTAL INFORMATION

Supplemental Information includes two figures and one table and can be found with this article online at http://dx.doi.org/10.1016/j.stemcr.2017.04.012.

AUTHOR CONTRIBUTIONS

M.N.F.M., A.G., K.B.S., A.H., and R.B. performed experiments and analyzed data. O.B. and H.C.C. provided *Ki67-RFP* mice. A.G. conceived the study and designed experiments. A.G. and A.R. wrote the manuscript.

ACKNOWLEDGMENTS

This work was supported by the German Research Foundation (DFG) through grant SFB 655 B11 to A.R., by the Excellence Initiative of the German Federal and State Governments "Support the best" (ZUK64, to A.R.), and TU Dresden Medical Faculty "MeDDrive 2015" grant to A.G. The authors thank Livia Schulze, Christa Haase, Tobias Häring, and Christina Hiller for expert technical assistance.

Received: December 13, 2016
Revised: April 11, 2017
Accepted: April 12, 2017
Published: May 11, 2017

REFERENCES

Balazs, A.B., Fabian, A.J., Esmon, C.T., and Mulligan, R.C. (2006). Endothelial protein C receptor (CD201) explicitly identifies hematopoietic stem cells in murine bone marrow. Blood *107*, 2317–2321.

Basak, O., van de Born, M., Korving, J., Beumer, J., van der Elst, S., van Es, J.H., and Clevers, H. (2014). Mapping early fate determination in Lgr5+ crypt stem cells using a novel KI67-RFP allele. EMBO J. *33*, 2057–2068.

Beerman, I., Bhattacharya, D., Zandi, S., Sigvardsson, M., Weissman, I.L., Bryder, D., and Rossi, D.J. (2010). Functionally distinct hematopoietic stem cells modulate hematopoietic lineage potential during aging by a mechanism of clonal expansion. Proc. Natl. Acad. Sci. USA *107*, 5465–5470.

Busch, K., Klapproth, K., Barile, M., Flossdorf, M., Holland-Letz, T., Schlenner, S.M., Reth, M., Höfer, T., and Rodewald, H.R. (2015). Fundamental properties of unperturbed haematopoiesis from stem cells in vivo. Nature *518*, 542–546.

de Bruin, A.M., Voermans, C., and Nolte, M.A. (2014). Impact of interferon-γ on hematopoiesis. Blood *124*, 2479–2486.

Dykstra, B., Kent, D., Bowie, M., McCaffrey, L., Hamilton, M., Lyons, K., Lee, S.J., Brinkman, R., and Eaves, C. (2007). Long-term propagation of distinct hematopoietic differentiation programs in vivo. Cell Stem Cell *1*, 218–229.

Eaves, C.J. (2015). Hematopoietic stem cells: concepts, definitions, and the new reality. Blood *125*, 2605–2613.

Egli, D., Rosains, J., Birkhoff, G., and Eggan, K. (2007). Developmental reprogramming after chromosome transfer into mitotic mouse zygotes. Nature *447*, 679–685.

Essers, M.A.G., Offner, S., Blanco-Bose, W.E., Waibler, Z., Kalinke, U., Duchosal, M.A., and Trumpp, A. (2009). IFNalpha activates dormant haematopoietic stem cells in vivo. Nature *458*, 904–908.

Foudi, A., Hochedlinger, K., Van Buren, D., Schindler, J.W., Jaenisch, R., Carey, V., and Hock, H. (2008). Analysis of histone 2B-GFP retention reveals slowly cycling hematopoietic stem cells. Nat. Biotechnol. *27*, 84–90.

Gough, D., Messina, N., Clarke, C., Johnstone, R., and Levy, D. (2012). Constitutive type I interferon modulates homeostatic balance through tonic signaling. Immunity *36*, 166–174.

Grinenko, T., Arndt, K., Portz, M., Mende, N., Günther, M., Cosgun, K.N., Alexopoulou, D., Lakshmanaperumal, N., Henry, I., Dahl, A., et al. (2014). Clonal expansion capacity defines two consecutive developmental stages of long-term hematopoietic stem cells. J. Exp. Med. *211*, 209–215.

Holmes, C., and Stanford, W.L. (2007). Concise review: stem cell antigen-1: expression, function, and enigma. Stem Cells *25*, 1339–1347.

Kamphuis, E., Junt, T., Waibler, Z., Forster, R., and Kalinke, U. (2006). Type I interferons directly regulate lymphocyte recirculation and cause transient blood lymphopenia. Blood *108*, 3253–3261.

Kiel, M.J., Yilmaz, Ö.H., Iwashita, T., Yilmaz, O.H., Terhorst, C., and Morrison, S.J. (2005). SLAM family receptors distinguish

hematopoietic stem and progenitor cells and reveal endothelial niches for stem cells. Cell *121*, 1109–1121.

Morita, Y., Ema, H., and Nakauchi, H. (2010). Heterogeneity and hierarchy within the most primitive hematopoietic stem cell compartment. J. Exp. Med. *207*, 1173–1182.

Müller-Sieburg, C.E., Cho, R.H., Thoman, M., Adkins, B., and Sieburg, H.B. (2002). Deterministic regulation of hematopoietic stem cell self-renewal and differentiation. Blood *100*, 1302–1309.

Oguro, H., Ding, L., and Morrison, S.J. (2013). SLAM family markers resolve functionally distinct subpopulations of hematopoietic stem cells and multipotent progenitors. Cell Stem Cell *13*, 102–116.

Okada, S., Nakauchi, H., Nagayoshi, K., Nishikawa, S., Miura, Y., and Suda, T. (1992). In vivo and in vitro stem cell function of C-KIT- and SCA-1-positive murine hematopoietic cells. Blood *80*, 3044–3050.

Osawa, M., Hanada, K., Hamada, H., and Nakauchi, H. (1996). Long-term lymphohematopoietic reconstitution by a single CD34-low/negative hematopoietic stem cell. Science *273*, 242–245.

Pietras, E.M., Lakshminarasimhan, R., Techner, J.-M., Fong, S., Flach, J., Binnewies, M., and Passegué, E. (2014). Re-entry into quiescence protects hematopoietic stem cells from the killing effect of chronic exposure to type I interferons. J. Exp. Med. *211*, 245–262.

Purton, L.E., and Scadden, D.T. (2007). Limiting factors in murine hematopoietic stem cell assays. Cell Stem Cell *1*, 263–270.

Qiu, J., Papatsenko, D., Niu, X., Schaniel, C., and Moore, K. (2014). Divisional history and hematopoietic stem cell function during homeostasis. Stem Cell Reports *2*, 473–490.

Sawai, C., Babovic, S., Upadhaya, S., Knapp, D., Lavin, Y., Lau, C., Goloborodko, A., Feng, J., Fujisaki, J., Ding, L., et al. (2016). Hematopoietic stem cells are the major source of multilineage hematopoiesis in adult animals. Immunity *45*, 597–609.

Säwén, P., Lang, S., Mandal, P., Rossi, D., Soneji, S., and Bryder, D. (2016). Mitotic history reveals distinct stem cell populations and their contributions to hematopoiesis. Cell Rep. *14*, 2809–2818.

Schoedel, K., Morcos, M., Zerjatke, T., Roeder, I., Grinenko, T., Voehringer, D., Göthert, J., Waskow, C., Roers, A., and Gerbaulet, A. (2016). The bulk of the hematopoietic stem cell population is dispensable for murine steady-state and stress hematopoiesis. Blood *128*, 2285–2296.

Shin, J.Y., Hu, W., Naramura, M., and Park, C.Y. (2014). High C-KIT expression identifies hematopoietic stem cells with impaired self-renewal and megakaryocytic bias. J. Exp. Med. *211*, 217–231.

Spangrude, G.J., Heimfeld, S., and Weissman, I.L. (1988). Purification and characterization of mouse hematopoietic stem cells. Science *241*, 58–62.

Sudo, T., Yokota, T., Oritani, K., Satoh, Y., Sugiyama, T., Ishida, T., Shibayama, H., Ezoe, S., Fujita, N., Tanaka, H., et al. (2012). The endothelial antigen ESAM monitors hematopoietic stem cell status between quiescence and self-renewal. J. Immunol. *189*, 200–210.

Sun, J., Ramos, A., Chapman, B., Johnnidis, J.B., Le, L., Ho, Y.J., Klein, A., Hofmann, O., and Camargo, F.D. (2014). Clonal dynamics of native haematopoiesis. Nature *514*, 322–327.

Vazquez, S.E., Inlay, M.A., and Serwold, T. (2015). CD201 and CD27 identify hematopoietic stem and progenitor cells across multiple murine strains independently of KIT and SCA-1. Exp. Hematol. *43*, 578–585.

Walter, D., Lier, A., Geiselhart, A., Thalheimer, F.B., Huntscha, S., Sobotta, M.C., Moehrle, B., Brocks, D., Bayindir, I., Kaschutnig, P., et al. (2015). Exit from dormancy provokes DNA-damage-induced attrition in haematopoietic stem cells. Nature *520*, 549–552.

Wiesmann, A., Phillips, R.L., Mojica, M., Pierce, L.J., Searles, A.E., Spangrude, G.J., and Lemischka, I. (2000). Expression of CD27 on murine hematopoietic stem and progenitor cells. Immunity *12*, 193–199.

Wilson, A., Laurenti, E., Oser, G., van der Wath, R.C., Blanco-Bose, W., Jaworski, M., Offner, S., Dunant, C.F., Eshkind, L., Bockamp, E., et al. (2008). Hematopoietic stem cells reversibly switch from dormancy to self-renewal during homeostasis and repair. Cell *135*, 1118–1129.

Wilson, N., Kent, D., Buettner, F., Shehata, M., Macaulay, I., Calero-Nieto, F., Sanchez Castillo, M., Oedekoven, C., Diamanti, E., Schulte, R., et al. (2015). Combined single-cell functional and gene expression analysis resolves heterogeneity within stem cell populations. Cell Stem Cell *16*, 712–724.

Yokota, T., Oritani, K., Butz, S., Kokame, K., Kincade, P.W., Miyata, T., Vestweber, D., and Kanakura, Y. (2008). The endothelial antigen ESAM marks hematopoietic stem cells throughout life. Blood *112*, 727.

Stem Cell Reports, Volume *8*

Supplemental Information

SCA-1 Expression Level Identifies Quiescent Hematopoietic Stem and Progenitor Cells

Mina N.F. Morcos, Kristina B. Schoedel, Anja Hoppe, Rayk Behrendt, Onur Basak, Hans C. Clevers, Axel Roers, and Alexander Gerbaulet

Figure S1

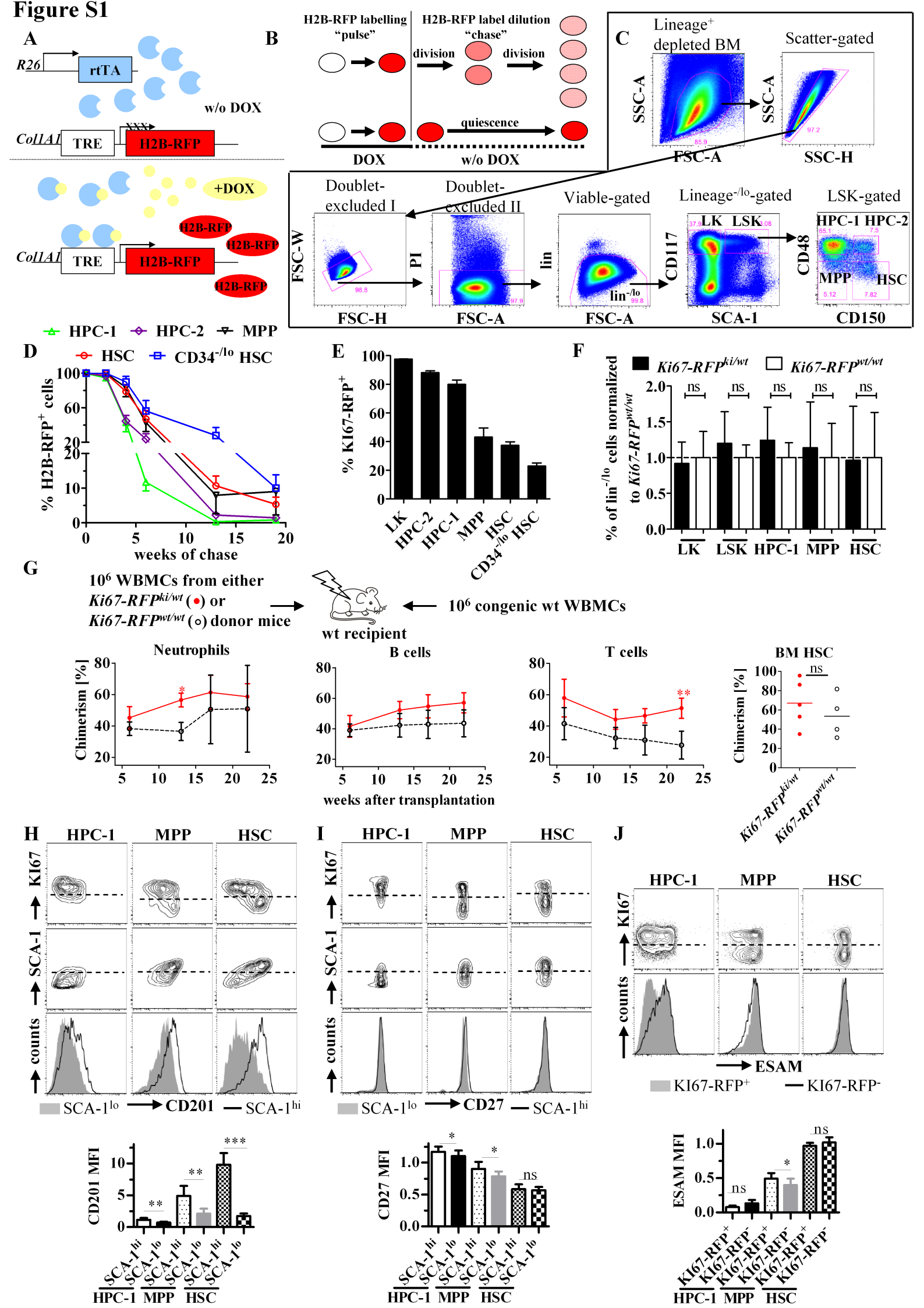
A
R26
rtTA
w/o DOX
Col1A1
TRE
H2B-RFP
+DOX
B
H2B-RFP labelling "pulse"
H2B-RFP label dilution "chase"
division
division
quiescence
DOX
w/o DOX
C
Lineage+ depleted BM
Scatter-gated
SSC-A
FSC-A
SSC-H
Doublet-excluded I
Doublet-excluded II
Viable-gated
Lineage-/lo-gated
LSK-gated
FSC-W
FSC-H
PI
lin
lin-/lo
CD117
LK
LSK
SCA-1
CD48
HPC-1
HPC-2
MPP
HSC
CD150
HPC-1
HPC-2
MPP
HSC
D
HSC
CD34-/lo HSC
% H2B-RFP+ cells
weeks of chase
E
% KI67-RFP+
LK
HPC-2
HPC-1
MPP
HSC
CD34-/lo HSC
F
Ki67-RFPki/wt
Ki67-RFPwt/wt
% of lin-/lo cells normalized to Ki67-RFPwt/wt
ns
LK
LSK
HPC-1
MPP
HSC
G
10⁶ WBMCs from either Ki67-RFPki/wt (•) or Ki67-RFPwt/wt (○) donor mice
10⁶ congenic wt WBMCs
wt recipient
Neutrophils
B cells
T cells
BM HSC
Chimerism [%]
weeks after transplantation
Ki67-RFPki/wt
Ki67-RFPwt/wt
H
HPC-1
MPP
HSC
KI67
SCA-1
counts
SCA-1lo
CD201
SCA-1hi
I
HPC-1
MPP
HSC
KI67
SCA-1
counts
SCA-1lo
CD27
SCA-1hi
J
HPC-1
MPP
HSC
KI67
counts
ESAM
KI67-RFP+
KI67-RFP-
CD201 MFI
CD27 MFI
ESAM MFI
SCA-1hi
SCA-1lo
HPC-1
MPP
HSC
KI67-RFP+
KI67-RFP-
ns

Figure S1. Mouse models for identification of quiescent hematopoietic stem and progenitor cells (related to Figure 1).

A Scheme of the *R26*^{rtTA}/*Col1A1*$^{H2B\text{-}RFP}$ mouse model. In the absence of doxycycline (DOX, yellow circles), the ubiquitously expressed reverse tetracycline transactivator (rtTA, blue circles) is unable to bind to tetracycline-responsive elements (TRE) of the TET-operon resulting in no or low level background expression of histone 2B-red fluorescent fusion protein (H2B-RFP). Systemic DOX administration results in massive induction of H2B-RFP (red ellipses) expression in all cells. **B** Scheme of H2B-RFP induction and dilution of the label by cell divisions. DOX induction leads to accumulation of H2B-RFP fusion protein ("pulse" period), while after DOX withdrawal ("chase") each cell division results in 50% dilution of H2B-RFP fluorescence. In contrast to this, non-dividing cells retain the H2B-RFP label. Note that the slow cell cycle-independent decay of the H2B-RFP protein was neglected in the scheme. **C** HSPC gating and sorting strategy adapted from Kiel et al., Cell, 2005. Representative dot plots of lineage-depleted WBMCs from a B6 wt mouse (LK, Lin$^{-/lo}$SCA-1^{-}CD117^{+}; LSK, Lin$^{-/lo}$SCA-1^{+}CD117^{+}; HPC-1, LSK CD48^{hi}CD150^{-}; HPC-2, LSK CD48^{hi}CD150^{+}; MPP, LSK CD48$^{-/lo}$CD150^{-}; HSC, LSK CD48$^{-/lo}$CD150^{+}; FSC, forward scatter; SSC, side scatter; PI, Propidium iodide; lin, hematopoietic lineage antigens). **D** *R26*^{rtTA}/*Col1A1*$^{H2B\text{-}RFP}$ mice (*R26* zygosity either *R26*$^{rtTA/wt}$ or *R26*$^{rtTA/rtTA}$, *Col1A1* zygosity either *Col1A1*$^{H2B\text{-}RFP/wt}$ or *Col1A1*$^{H2B\text{-}RFP/H2B\text{-}RFP}$) were DOX-pulsed for 8 weeks, chased for 0 (n=3), 2 (n=1), 4 (n=2), 6 (n=4), 13 (n=8) or 19 (n=9) weeks and BM was analyzed by flow cytometry for retention of H2B-RFP. Mean frequencies of H2B-RFP^{+} cells (± SD) among HSPC populations are shown (for gating see Figure S1C; CD34$^{-/lo}$ HSC, LSK CD48$^{-/lo}$CD150^{+}CD34$^{-/lo}$). The H2B-RFP^{+} gate was set using *R26*^{wt}/*Col1A1*$^{H2B\text{-}RFP}$ mice in order to control for the low level of background H2B-RFP expression from the *Col1A1*$^{H2B\text{-}RFP}$ allele.

E Mean frequencies (± SD) of KI67-RFP^{+} cells among BM HSPCs isolated from *Ki67-RFP*$^{ki/wt}$ mice (n=4) were analyzed by flow cytometry (KI67-RFP^{+} gate was set according to *Ki67-RFP*$^{wt/wt}$ controls; for HSPC gating see Figure S1C; CD34$^{-/lo}$ HSC, LSK CD48$^{-/lo}$CD150^{+}CD34$^{-/lo}$).

F BM HSPC population size of *Ki67-RFP*$^{ki/wt}$ (n=4) and *Ki67-RFP*$^{wt/wt}$ (n=3) mice was determined (mean frequencies (± SD) among lineage depleted BM cells are shown, mean frequencies of *Ki67-RFP*$^{wt/wt}$ mice were normalized to 1 (dotted line), significance was calculated by unpaired Student´s t-test with Bonferroni-Holm error correction).

G 10^6 WBMCs from either *Ki67-RFP*$^{ki/wt}$ (red circles) or *Ki67-RFP*$^{wt/wt}$ (black circles) mice were each mixed with 10^6 competitor B6.CD45.1 WBMCs and transplanted into lethally irradiated B6.CD45.1/.2 recipients (n=4-5 / per donor genotype). PB neutrophil, B- and T-lymphocyte chimerism was analyzed (mean ± SD are shown, significance was calculated with repeated measure two way ANOVA and Bonferroni error correction, only significant results are indicated). BM HSC (LSK CD48$^{-/lo}$CD150^{+}) chimerism of recipient mice was analyzed 23 weeks after transplantation (individual mice and means (bars) are shown, significance was calculated by unpaired Student´s t-test).

H BM of *Ki67-RFP*$^{ki/wt}$ mice (n=6) was analyzed by flow cytometry. Representative contour plots of HPCs-1 (LSK CD48^{hi}CD150^{-}), MPPs (LSK CD48$^{-/lo}$CD150^{-}) and HSCs (LSK CD48$^{-/lo}$CD150^{+}) are shown. Upper row depicts CD201 (EPCR) against KI67-RFP expression (dotted lines show threshold for KI67-RFP gating, set according to *Ki67-RFP*$^{wt/wt}$ control). Middle row shows CD201 against SCA-1 expression (dotted lines show threshold for arbitrary SCA-1^{hi} and SCA-1^{lo} gating). Lower row displays representative histograms of CD201 expression by either SCA-1^{lo} (solid grey histograms) or SCA-1^{hi} (black lines) cells among the respective parental HSPC population. Lower data plot quantifies CD201 expression of HSPC populations separated by SCA-1 expression level. CD201 MFI was normalized to the mean MFI of the total LSK population, which was set to 1 (means ± SD are shown, significance was calculated by paired Student´s t-test and Bonferroni-Holm error correction).

I BM of *Ki67-RFP*$^{ki/wt}$ mice (n=6) was analyzed by flow cytometry for expression of CD27 among HSPCs. Display, normalization and statistical analysis of data was performed as in Figure S1H.

J BM of *Ki67-RFP*$^{ki/wt}$ mice (n=4) was analyzed by flow cytometry for ESAM and KI67-RFP expression. Representative contour plots of HPCs-1 (LSK CD48^{hi}CD150^{-}), MPPs (LSK CD48$^{-/lo}$CD150^{-}) and HSCs (LSK CD48$^{-/lo}$CD150^{+}) are shown (upper row, dotted lines show threshold for KI67-RFP gating). Lower row compares ESAM expression between KI67-RFP^{+} (solid grey histograms) and KI67-RFP^{-} (black lines) cells among the respective parental population. Lower data plot depicts ESAM expression of HSPC populations separated by KI67-RFP expression. ESAM MFI was normalized to the mean MFI of the total HSC population, which was set to 1 (mean ± SD are shown, significance was calculated by paired Student´s t-test and Bonferroni-Holm error correction).

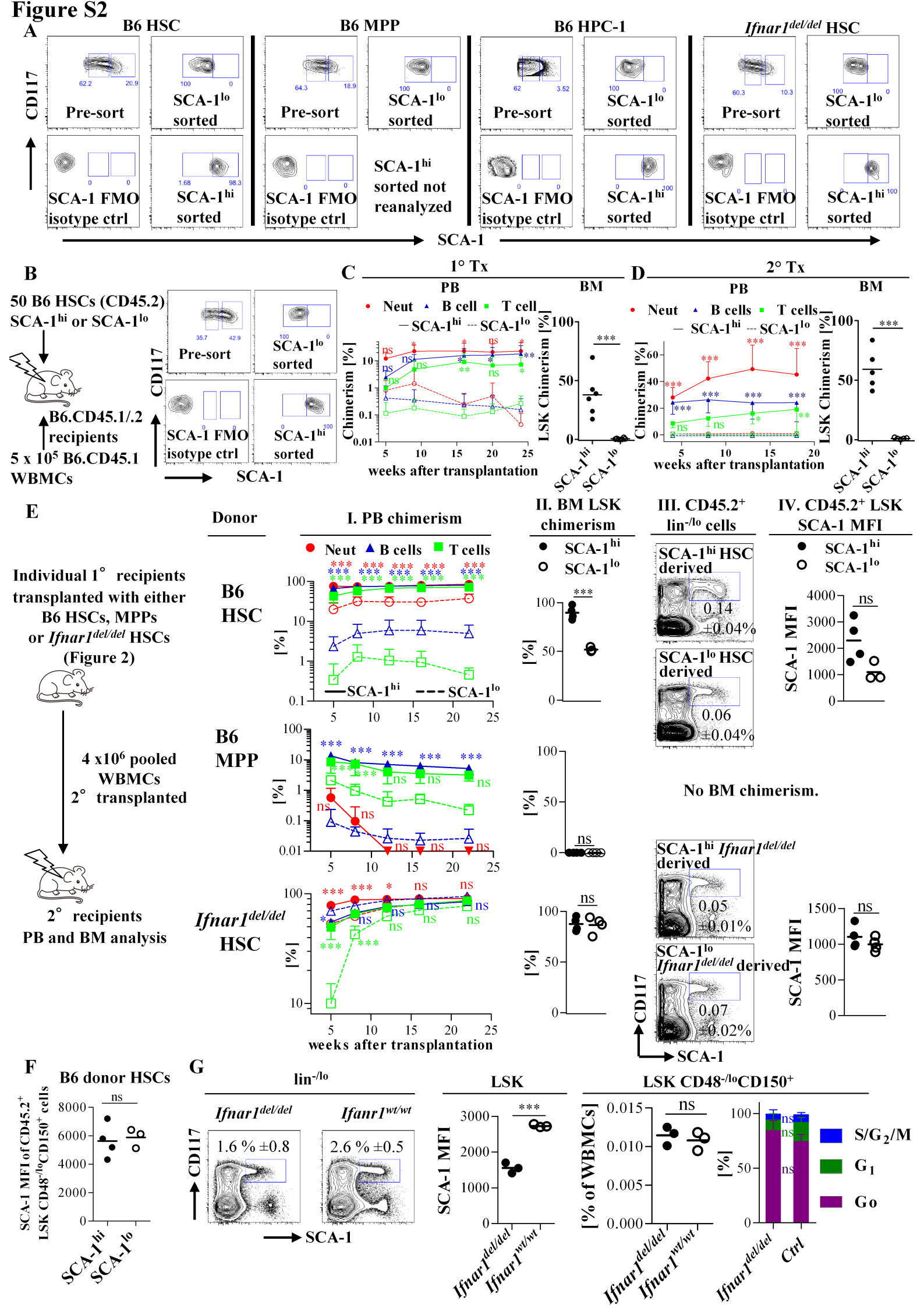
Figure S2
A
B6 HSC
B6 MPP
B6 HPC-1
Ifnar1del/del HSC
CD117
Pre-sort
SCA-1lo sorted
SCA-1 FMO isotype ctrl
SCA-1hi sorted
SCA-1hi sorted not reanalyzed
SCA-1
B
50 B6 HSCs (CD45.2)
SCA-1hi or SCA-1lo
B6.CD45.1/.2 recipients
5 x 10^5 B6.CD45.1 WBMCs
C
1° Tx
PB
BM
Neut
B cell
T cell
SCA-1hi
SCA-1lo
Chimerism [%]
LSK Chimerism [%]
weeks after transplantation
D
2° Tx
E
Donor
I. PB chimerism
II. BM LSK chimerism
III. CD45.2+ lin-/lo cells
IV. CD45.2+ LSK SCA-1 MFI
Individual 1° recipients transplanted with either B6 HSCs, MPPs or Ifnar1del/del HSCs (Figure 2)
B6 HSC
B6 MPP
Ifnar1del/del HSC
4 x10^6 pooled WBMCs 2° transplanted
2° recipients PB and BM analysis
SCA-1hi HSC derived
SCA-1lo HSC derived
0.14 ±0.04%
0.06 ±0.04%
No BM chimerism.
SCA-1hi Ifnar1del/del derived
SCA-1lo Ifnar1del/del derived
0.05 ±0.01%
0.07 ±0.02%
SCA-1 MFI
F
B6 donor HSCs
SCA-1 MFI of CD45.2+ LSK CD48-/loCD150+ cells
G
lin-/lo
LSK
LSK CD48-/loCD150+
Ifnar1del/del
Ifanr1wt/wt
1.6 % ±0.8
2.6 % ±0.5
[% of WBMCs]
S/G2/M
G1
Go
Ctrl

Figure S2. Purification and transplantation of hematopoietic stem and progenitor cells according to SCA-1 expression levels (related to Figure 2).

A Contour plots show purification and reanalysis of either SCA-1^{hi} or SCA-1^{lo} HSPC donor populations transplanted in the experiment shown in Figure 2. SCA-1 Fluorescence-minus-one (FMO) isotype controls confirmed that all sorted populations were indeed SCA-1^{+}. Reanalysis of the SCA-1^{hi} sorted MPP population was not performed due to recovery of an insufficient cell number.

B B6 HSCs (LSK CD48$^{-/lo}$CD150^{+}) were fractionated according to SCA-1 expression and 50 cells were transplanted together with 5x10^{5} B6.CD45.1 competitor WBMCs into lethally irradiated B6.CD45.1/.2 recipients. Contour plots show purification and reanalysis of SCA-1^{hi} or SCA-1^{lo} donor HSCs,

C PB chimerism of primary (1° Tx) recipient mice (n= 6 / group, shown in Figure S2B) was monitored longitudinally (red circles, neutrophils; blue triangles, B cells; green boxes, T cells, continuous lines SCA-1^{hi} donor HSCs, dotted lines SCA-1^{lo} donor HSCs, means ± SD are shown, significance was calculated with repeated measure two way ANOVA with Bonferroni error correction). BM analysis of recipient mice revealed LSK donor chimerism (individual recipients and means are shown, unpaired Student´s t-test).

D 4x10^{6} WBMCs from pooled 1° recipient mice shown in Figure S2C were secondarily transplanted (2° Tx) into lethally irradiated recipients (n=5 / group) and PB and BM LSK chimerism (as in S2C) were analyzed.

E 4x10^{6} pooled WBMCs from 1° recipient mice from the experiment shown in Figure 2 were secondarily transplanted (2° Tx) into lethally irradiated recipients (n=3-4/group). Display and analysis of secondary recipient data is similar to Figure 2. **Column I.** depicts PB chimerism analysis (red circles, neutrophils; blue triangles, B cells; green boxes, T cells, continuous lines SCA-1^{hi} donor cells, dotted lines SCA-1^{lo} donor cells, means ± SD are shown, significance was calculated with repeated measure two way ANOVA with Bonferroni error correction). 2° transplantation of recipients that received SCA-1^{lo} MPP donor cells did not result in detectable neutrophil chimerism, while 2° recipients of SCA-1^{hi} MPP transplanted mice initially displayed low neutrophil chimerism, but neutrophil reconstitution was completely lacking after 12 weeks of 2° transplantation (indicated by inverted triangles on x-axis). **Column II.** depicts BM LSK chimerism of secondary recipients (individual mice and means are shown, unpaired Student´s t test). **Column III.** shows representative examples of contour plots of donor-derived (CD45.2^{+}) lin$^{-/lo}$ cells (mean frequencies ± SD of CD45.2^{+} LSK cells among total WBMCs are shown). **Column IV.** depicts SCA-1 MFI of donor-derived LSK cells (individual secondary recipients and means are shown, unpaired Student´s t test).

F SCA-1 MFI of the donor-derived (CD45.2^{+}) HSCs isolated from primary recipients (shown in Figure 2), which were transplanted with B6 HSCs, was analyzed (individuals and means are displayed, unpaired Student´s t test).

G WBMCs isolated from *Ifnar1*$^{del/del}$ or *Ifnar1*$^{wt/wt}$ mice (n=3/genotype) were analyzed by flow cytometry. The frequency of LSK cells among lin$^{-/lo}$ population (left, representative contour plots, mean ±SD) is displayed. SCA-1 MFI of LSK cells (middle data plot, individual mice and means, significance assessed by unpaired Student´s t test) was determined. The frequency of LSK CD48$^{-/lo}$CD150^{+} cells among WBMCs was unchanged in *Ifnar1*$^{del/del}$ mice compared to *Ifnar1*$^{wt/wt}$ controls (right data panel, individual mice and means are shown, significance calculated by unpaired Student´s t test). The proportion of LSK CD48$^{-/lo}$CD150^{+} cells in different cell cycle phases (G_0, G_1, S/G_2/M) in *Ifnar1*$^{del/del}$ (n=5) and control mice (genotype either *Ifnar1*$^{wt/del}$ *or Ifnar1*$^{wt/wt}$, n=4) was analyzed (mean ± SD, significance calculated by unpaired Student´s t test with Bonferroni-Holm error correction).

Table S1

Epitope	*Clone*	*Manufacturer*
CD117	2B8, 3C11	eBioscience, Miltenyi
CD11b	M1/70	eBioscience
CD135	A2F10	eBioscience
CD150	TC15-12F12.2	Biolegend
CD16/32	93	Biolegend
CD19	eBio1D3	eBioscience
CD27	LG.3A10	Biolegend
CD201 (EPCR)	eBio1560	eBioscience
CD34	RAM34	eBioscience
CD3e	145-2C11, eBio500A2	eBioscience
CD4	GK1.5	eBioscience
CD45.1	A20	eBioscience
CD45.2	104	eBioscience
CD45R (B220)	RA3-6B2	eBioscience
CD48	HM48-1	BD Biosciences
CD8a	53-6.7	eBioscience
ESAM	1G8/ESAM	Biolegend
GR-1 (LY-6C/G)	RB6-8C5	eBioscience
KI67	B56	BD Biosciences
NK1.1	PK136	eBioscience
SCA-1 (LY-6A/E)	D7	eBioscience
TER119	TER-119	eBioscience

Table S1
Overview of monoclonal antibodies used for flow cytometry.